Applied Catalysis B: Environmental 192 (2016) 46–56

Contents lists available at ScienceDirect

Applied Catalysis B: Environmental

journal homepage: www.elsevier.com/locate/apcatb

Amorphous $Fe_{78}Si_9B_{13}$ alloy: An efficient and reusable photo-enhanced Fenton-like catalyst in degradation of cibacron brilliant red 3B-A dye under UV–vis light

Z. Jia [a], W.C. Zhang [b], W.M. Wang [c], D. Habibi [a], L.C. Zhang [a,*]

[a] School of Engineering, Edith Cowan University, 270 Joondalup Drive, Joondalup, Perth, WA 6027, Australia
[b] Environmental Protection Administration of Ji'an City, Ji'an, Jiangxi Province 343000, China
[c] School of Materials Science and Engineering, Shandong University, Jinan, Shandong 250061, China

ARTICLE INFO

Article history:
Received 19 January 2016
Received in revised form 11 March 2016
Accepted 22 March 2016
Available online 23 March 2016

Keywords:
Catalyst
Amorphous $Fe_{78}Si_9B_{13}$ alloy
Photo-enhanced
Reaction kinetics

ABSTRACT

The development of new functional applications of amorphous alloy is an active and challenging topic. In this work, amorphous $Fe_{78}Si_9B_{13}$ alloy, a photo-enhanced Fenton-like catalyst, exhibits excellent functional ability in degrading an azo dye. This study reports the dramatic performance gains achieved for photo-enhanced Fenton-like degradation of cibacron brilliant red 3B-A (BR3B-A) dye aqueous solutions, the reusability of amorphous $Fe_{78}Si_9B_{13}$ alloy ribbon catalysts, and the reaction kinetics (k) of the process. The individual and synthetical effects of the various reaction parameters are investigated by employing an orthogonal matrix ($L_{16}(4^5)$) experimental methodology. The investigation evaluates the impact of these parameters on the degradation process, in order to demonstrate that UV–vis light could continuously induce hydroxyl radicals (•OH) to be generated in the dye aqueous solution and significantly enhance the rate of dye degradation and mineralization. The experimental results show that nearly 100% color removal is achieved within 5 min under conditions of 2.0 g/L $Fe_{78}Si_9B_{13}$ ribbons, 0.5 M H_2O_2 and pH 2. UV–vis light intensity ranging from 0 to 7.7 μW/cm^2 enhances a dramatic improvement in color removal from 78% at 200 min to 98% at 60 min and an improvement in the reaction kinetics (k) from 0.0413 at 0 μW/cm^2 of light irradiation to 0.2901 at 7.7 μW/cm^2 of light irradiation under conditions of 2.0 g/L $Fe_{78}Si_9B_{13}$ ribbons, 0.5 M H_2O_2 and natural pH 6.45. The production of •OH is investigated by adding tertiary butanol, resulting in a sharp decrease of dye color removal. Structural characterizations of as-received amorphous $Fe_{78}Si_9B_{13}$ ribbons and of recycled $Fe_{78}Si_9B_{13}$ ribbons are also investigated by transmission electron microscopy (TEM), X-ray diffraction (XRD), UV–vis diffuse reflectance spectrophotometers (UV–vis DRS), scanning electron microscope (SEM) and energy-dispersive X-ray spectroscopy (EDS); the results reveal a slight decay of the reused $Fe_{78}Si_9B_{13}$ ribbons, along with a gradual precipitation of crystallized α-Fe, iron oxide and SiO_2 on the ribbon surface over the few cycles of usage.

1. Introduction

Amorphous alloys, also alternatively known as metallic glasses, are made by processing the intrinsic crystalline structure into short-range ordered and long-range disordered atomic structure. Their superior properties and industrial applications have been attracting increased attention from many researchers. For example, Co- and Ni-based amorphous alloys are employed in core transformers because of their excellent properties [1]. Ni-based amorphous alloys are utilized as coating materials as a result of their superior wear resistance and corrosion resistance [2]. Fe-based amorphous alloys exhibit a particular beneficial combination of soft magnetic properties and excellent oxidation characteristics. Recently, thanks to their unique physical, chemical, and mechanical properties, amorphous alloys are also regarded to be potential catalysts for degrading dye pollutions [3,4].

In the search for an effective technique for the purification of dye polluted water, various processes aimed specifically at facilitating the degradation of the dye effluent have been proposed. Some most prominent processes are membrane separation [5], chemical

Abbreviations: BR3B-A, cibacron brilliant red 3B-A; EDS, energy-dispersive X-ray spectroscopy; SEM, scanning electron microscope; TEM, transmission electron microscopy; TOC, total organic carbon; UV–vis DRS, UV–visible diffuse reflectance spectrophotometers; XRD, X-ray diffraction.

* Corresponding author.
E-mail addresses: l.zhang@ecu.edu.au, lczhangimr@gmail.com (L.C. Zhang).

http://dx.doi.org/10.1016/j.apcatb.2016.03.048
0926-3373/

coagulation [6,7], activated carbon adsorption [8,9], photocatalytic degradation [10,11], and Fenton catalytic decomposition [12–15]. Among these processes, the use of crystalline zero-valent iron (ZVI) as a catalyst in the heterogeneous Fenton method has attracted significant industrial interest, largely because of the low cost, high dye degradation efficiency, and simple operation [16–18]. The most important drawback to the Fenton method is the rapid decay of the catalyst because of corrosion [19]. To date, in order to overcome these disadvantages of the traditional Fenton process, three types of materials have been recently received extensive attention, such as natural Fe containing catalysts (limonite and goethite) [20], iron-oxygen compounds (α-Fe_2O_3 and α-FeOOH [21], Fe_3O_4 [22] *etc.*) and the catalysts of immobilizing Fe (carbon-Fe [23], Fe-loaded resin [24], clay-based Fe [25] *etc.*). These Fenton or Fenton-like catalysts demonstrate a wider pH range for degrading various organic substances, but many of them do not show a favorable efficiency for degrading organic pollutions. Very recently, Fe-based amorphous alloys are reported as an advanced catalyst for wastewater degradation mainly owning to the following three particular properties: (1) the elements do not reside at the thermodynamic equilibrium positions, it is possible to tune and optimize the properties of the amorphous alloys by manipulating their chemical composition [26–28], (2) the constituent atoms are located far from their equilibrium states, thus, the amorphous alloy still exhibits advanced properties even in micro- or nano-scale, subsequently, surface to volume ratio is easily to be tuned without changing properties [19,29,30], (3) the metastable nature, compared to crystalline material, the amorphous alloy has higher Gibbs free energy [31,32].

Azo dyes are distinguished by the presence of at least one azo group (—N═N—). They are commonly used in the textile industry for decorative and other similar purposes. Since as a consequence of their characteristic lengths and shapes they are a type of very effective dyes when used with cellulose fibers [33]. However, azo dyes have a serious drawback as they exhibit a number of toxicities due to the following reasons. First, they are precursors to various known carcinogens (the carcinogenic amino groups and para-isomers are the main components of azo dyes [34]). Second, toxic aromatic amines are produced in aqueous dye solutions following the cleaving of the azo linkage [35]. Toxic aromatic amines are very difficult to remove from aqueous solutions, and in addition, they have a deleterious impact on the environment as a whole, in particular on human health. Third, highly reactive, very harmful electrophilic diazonium salts are produced after the direct oxidation of the azo linkage in azo dyes [36]. The color presence of these azo dyes in the effluent outfall from textile plants using these dyes is also a highly problematic environmental issue. Only a minute amount of azo dye in the effluent stream is enough to make startling color change in a body of water. Moreover, these colorants deteriorate the adsorption and reflection of the sunlight, resulting in the unregulated rise of bacterial colonies in the contaminated water [37].

Cibacron brilliant red 3B-A (BR3B-A), *i.e.* reactive red 4 dye ($C_{32}H_{24}ClN_8Na_4O_{14}S_4$, tetrasodium 5-(benzoylamino)-3-[[5-[[4-chloro-6-[(4-sulphonatophenyl)amino]-1,3,5-triazin-2-yl]amino]-2-sulphonatophenyl]azo]-4-hydroxynaphthalene-2,7-disulphonate), has been employed in dyeing processes because of their desirable properties including strong interaction with substrate, bright color, water-fastness, simple application techniques, and lower energy consumption required for dyeing process. This work investigated the degradation efficiency of the photo-enhanced Fenton-like process and the reaction kinetics of BR3B-A dye in aqueous solution by using advanced amorphous $Fe_{78}Si_9B_{13}$ alloy as catalysts. An orthogonal design matrix ($L_{16}(4^5)$) was utilized to develop an experimental methodology for studying the dye degradation efficiency. It is well known that the specific reaction parameters of interest for the dye degradation process are initial dye concentration, H_2O_2 concentration, catalyst dosage, initial pH value, and irradiation intensity. The effect of each of these reaction parameters on the dye degradation and mineralization process was studied in detail. The conductivity of the dye solution was continuously monitored during the UV–vis light irradiation, as an indicator of the progress of the photo-enhanced Fenton-like dye degradation reactions. Tertiary butanol was employed for the investigation of the production of •OH. In addition, the degradation efficiency and reaction kinetics (k) of the recycled amorphous $Fe_{78}Si_9B_{13}$ alloy were investigated in detail. The mechanisms for the decay of the catalyst were also studied by TEM, XRD, UV–vis DRS, SEM and EDS.

Table 1
Structure and characteristics of BR3B-A dye.

Structure	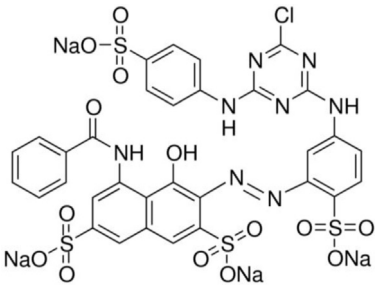
Empirical formula	$C_{32}H_{24}ClN_8Na_4O_{14}S_4$
Molecular Weight	1000.25
λ_{max} (nm)	517

2. Materials and methods

2.1. Chemicals

The BR3B-A dye was supplied by Sigma-Aldrich (Product Number: 228451). Some general physical characteristics of the dye are summarized in Table 1. Amorphous alloy ribbons having the nominal composition of $Fe_{78}Si_9B_{13}$ and with 40–60 μm thick were manufactured by melt-spinning under argon atmosphere. The as-spun amorphous alloy ribbons were cut into pieces with 5 × 20 mm as catalysts. Analytical grade H_2O_2 (30 wt%), was purchased from Chem-Supply. Milli-Q water of 18.2 MΩ cm was employed throughout for all aqueous solutions, as a component of the mixed water and dye solutions. Other chemicals such as $C_4H_{10}O$ (tertiary butanol), NaOH and HCl were all of analytical grade, not requiring further purification.

2.2. Methods

In the dye degradation experiments, specific amounts of the amorphous alloy ribbons were placed into a 100 mL dye aqueous solution containing specific concentration of H_2O_2. The various dye solutions were stirred by Vortex-Genie 2 mixer (Scientific Industries, Inc. USA) and irradiated under a 300 W Xeon simulated solar light lamp (Perfectlight Scientific Pty Ltd., Beijing, China). Samples were taken at the predetermined time intervals (*i.e.* 1, 2, 5, 10, 15, 30, 45, and 60 min). All the samples were processed by flocculation – centrifugation (Sigma, Germany) – filter (Pall Corporation, New York, USA) method in order to avoid further degradation of the sample in the tubes. Each dye solution sample was characterized in turn by the use of a Perkin Elmer Lambda 35 UV–vis spectrometer (Shelton, CT, USA). The TOC of the dye aqueous solution was determined with a TOC-5000CE analyzer (Shimadzu, Japan). The

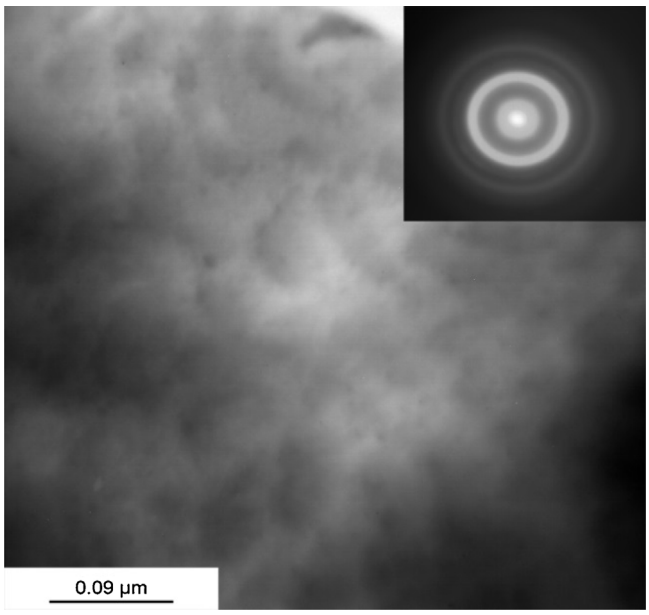

Fig. 1. The TEM image and SAED pattern (inset) of the as-received $Fe_{78}Si_9B_{13}$ amorphous ribbons.

wavelength of light absorbance λ_{max} was measured to be 517 nm. Dye degradation efficiency was calculated by:

$$X = (C_0 - C)/C_0 \times 100\% \quad (1)$$

where C_0 and C are the initial concentration and the concentration at time t of BR3B-A dye, respectively.

The structural features of the as-received amorphous $Fe_{78}Si_9B_{13}$ ribbons were examined by TEM using a JEOL JEM-2010 microscope (Tokyo, Japan) and XRD using a PANalytical Empyrean diffractometer with monochromated Co-Kα radiation at ambient temperature. The surface morphology of the ribbons before and after degradation was determined by UV–vis DRS (Shelton, CT, USA) and SEM equipped with EDS (JEOL 6000, Japan) with an accelerating voltage of 15 kV. The recycled ribbon samples were first washed with Milli-Q water in an ultrasonic cleaner for 3 min, after which the surface of the recycled ribbons were further cleaned by analytical grade alcohol. All the treated ribbon samples were preserved by sealing in the experimental container.

3. Results and discussions

3.1. Characterizations of $Fe_{78}Si_9B_{13}$ ribbons

Fig. 1 shows a TEM image and the corresponding selected area electron diffraction (SAED) pattern (inset) of the as-received $Fe_{78}Si_9B_{13}$ ribbons. It is noted that the $Fe_{78}Si_9B_{13}$ alloy ribbons are mainly amorphous with trace of small crystalline precipitates of Fe_3B and α-Fe [38]. Fig. 2(a) shows the XRD patterns for the as-received and also the recycled $Fe_{78}Si_9B_{13}$ ribbons. All the samples exhibit a broad diffuse diffraction peak at $2\theta = 40–60^\circ$ in the corresponding XRD pattern, indicating that the structure of the ribbons are mainly in amorphous state [39–43]. It is noted that the intensities of main diffraction peaks exhibited by the ribbons move to a higher diffraction angle after increasing the number of times that the ribbons had been reused, *i.e.* from 2008 (counts.) and 262 (counts.) for the as-received ribbons to 4110 (counts.) and 490 (counts.) for the 4th run ribbons at $2\theta = 52.5^\circ$ and 96°, respectively. It is confirmed that crystallized α-Fe is formed on the surface of the $Fe_{78}Si_9B_{13}$ ribbons under UV–vis light irradiation, after being employed as a catalyst for degrading the BR3B-A dye [44,45]. Fig. 2(b) shows the UV–vis DRS characterization of the as-received amorphous $Fe_{78}Si_9B_{13}$ ribbons and 1st run recycled $Fe_{78}Si_9B_{13}$ ribbons. It is confirmed that the isolated iron species are attributed to the bands between 200 and 300 nm, either tetrahedrally coordinated, or octahedrally coordinated [46,47]. The bands between 300 and 450 nm indicate that the octahedral irons are in the form of $Fe^{3+}{}_xO_y$ complexes, while bands at a wavelength greater than 450 nm are typically attributed to large iron oxide aggregates [46,47]. It is noted that the as-received $Fe_{78}Si_9B_{13}$ ribbons present two main peaks in the band between 200 and 400 nm and there is no apparent peak after 450 nm; which indicates that the iron species in the as-received $Fe_{78}Si_9B_{13}$ ribbons are distributed homogeneously, and there is no iron oxide aggregates on the ribbon surface. In contrast to the result for the as-received $Fe_{78}Si_9B_{13}$ ribbons, the 1st run recycled $Fe_{78}Si_9B_{13}$ ribbons show a significant peak which is at greater than 450 nm, indicating that iron oxide aggregates (excepting α-Fe) are also precipitated on the surface of recycled ribbons. In addition, a main peak in the 250–300 nm band indicates that the isolated iron species on the 1st run recycled ribbons can still degrade the dye efficiently.

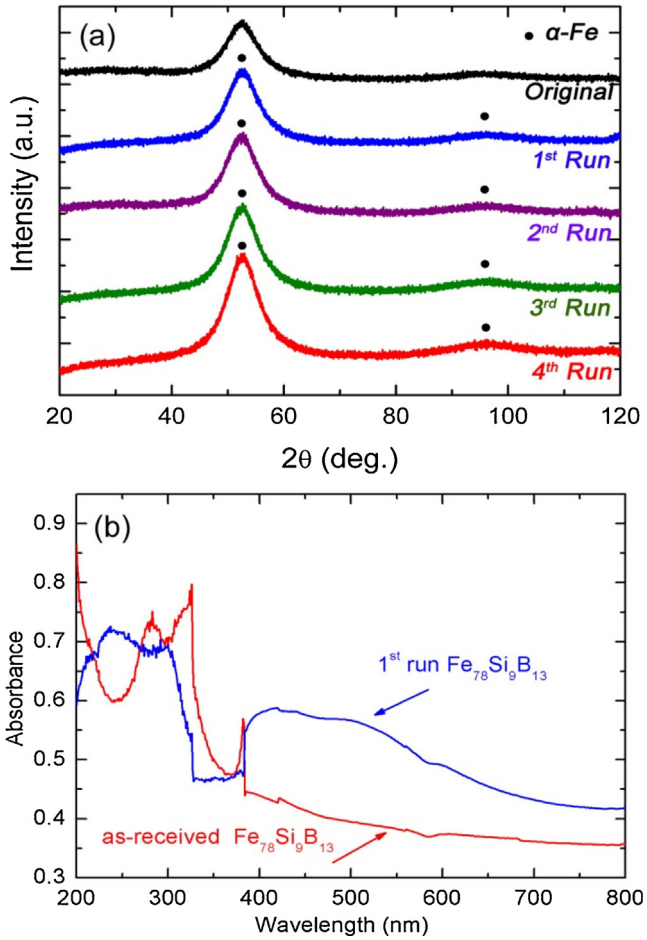

Fig. 2. (a) XRD patterns and (b) UV–vis DRS of the as-received amorphous $Fe_{78}Si_9B_{13}$ ribbons and of recycled $Fe_{78}Si_9B_{13}$ ribbons after multiple runs (dye concentration: 20 ppm, natural pH 6.45, $Fe_{78}Si_9B_{13}$ dosage: 2.0 g/L, H_2O_2 concentration: 0.5 M, irradiation intensity: 7.7 μW/cm^2).

Fig. 3(a) and (b) show the SEM micrograph and EDS image of the as-received $Fe_{78}Si_9B_{13}$ ribbons. It can be seen that the free surface of the as-received $Fe_{78}Si_9B_{13}$ ribbons is nearly smooth, and the atom ratio of Si to Fe for the as-received $Fe_{78}Si_9B_{13}$ ribbons is approximately 1:9, where Si is (10.14%) and Fe is (89.86%). Consequently, it can be seen that the atom ratio of Si to Fe on the surface of the

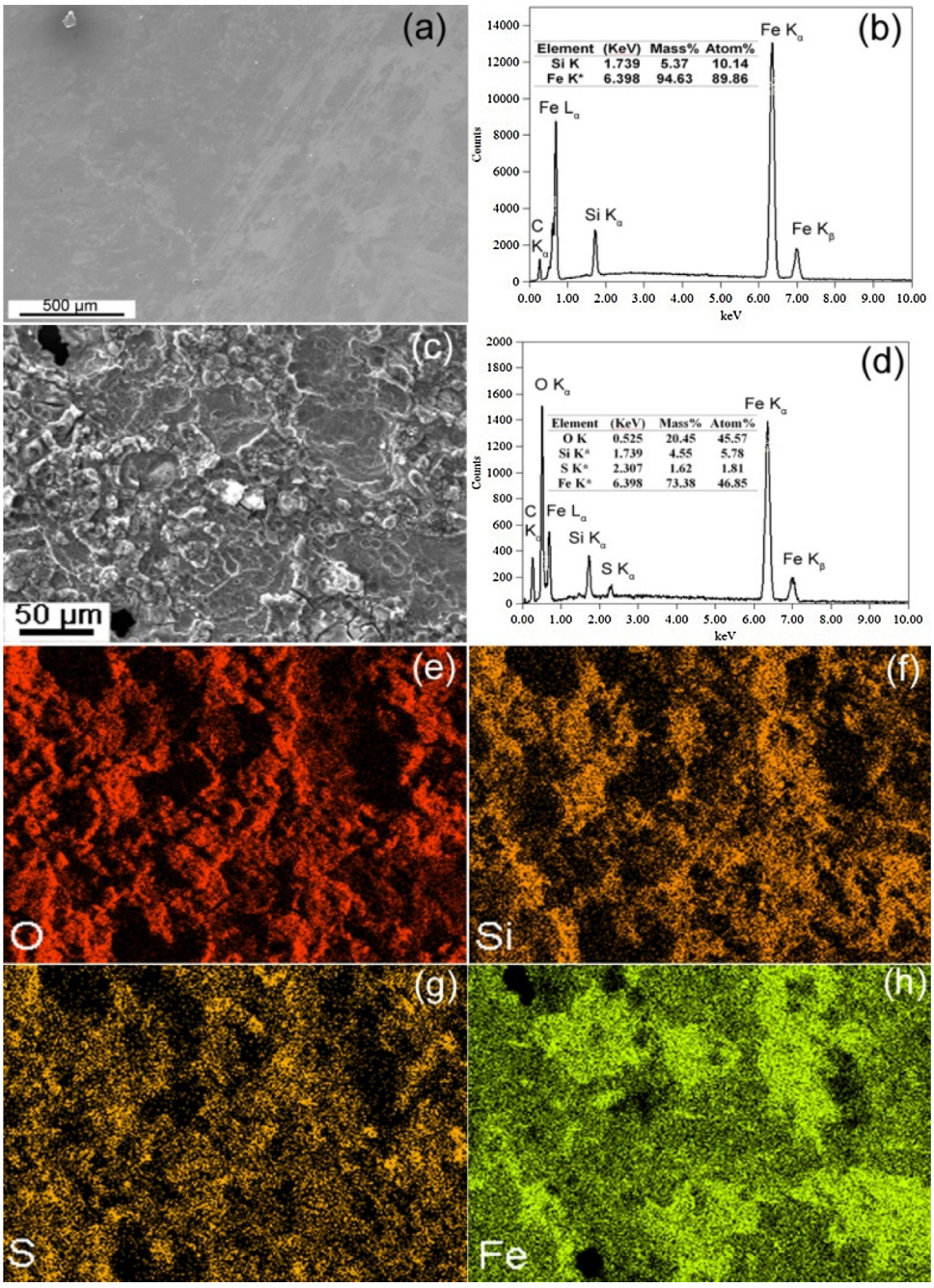

Fig. 3. (a) SEM micrograph and (b) EDS result of as-received $Fe_{78}Si_9B_{13}$ ribbons, (c) SEM image, (d) EDS result and (e)–(h) EDS mapping results of 1st run recycled $Fe_{78}Si_9B_{13}$ ribbons.

material is very close to the nominal value expected for the $Fe_{78}Si_9B_{13}$ catalyst, which is the ratio of 9:78. However, it is found that the presence of Fe and Si on the surface of the used $Fe_{78}Si_9B_{13}$ ribbons is sharply reduced, while the amount of C, O, and S all increase (Fig. 3(b), (d), (e) and (g)). The decrease in the amount of Fe confirms that the dye degradation is a result of the Fe having reacted with the H_2O_2 to produce hydroxyl radicals (•OH), which in turn causes an aggressive oxidation of the dye molecules. During the dye degradation reaction, Si (in the form of SiO_2) precipitates on the surface of the recycled ribbons. Fortunately the SiO_2 falls easily from the surface whilst being stirred by the Vortex stirrer, enabling more contact area to be quickly provided between the previously buried Fe atoms and the H_2O_2 molecules. It is also interesting to notice that the distribution of Fe on the recycled ribbons is more concentrated in the troughs on the surface of the ribbon. These troughs are the regions of higher activity, where the SiO_2 has been previously generated and then removed. The presence of the large number of O atoms confirms the formation of iron oxide and silicon oxide on the surface, and is in good agreement with Fig. 2b. The appearance of C and S atoms on the surface of the ribbon indicate that the dye molecules have been degraded and mineralized, and that the final products have been adsorbed on the ribbons surface.

3.2. Establishment of the experimental design matrix using factorial design

The Fenton-like dye color removal process and the degradation rate of the $Fe_{78}Si_9B_{13}$ ribbons are strongly influenced by the

Table 3
Results of experimental orthogonal arrays ($L_{16}(4^5)$) for reaction kinetics (k).

		K[a]	K_{avg}	Range analysis (R)
Dye concentration (ppm)	10	0.5863	0.1465	0.1680
	20	0.9204	0.2301	
	50	1.2580	0.3145	
	100	0.6842	0.1710	
Catalyst dosage (g/L)	0.2	0.6965	0.1741	0.0621
	0.5	0.8812	0.2203	
	1.0	0.9261	0.2315	
	2.0	0.9451	0.2362	
H_2O_2 concentration (M)	0.2	0.5473	0.1368	0.1625
	0.5	1.1972	0.2993	
	0.8	1.0157	0.2539	
	1.0	0.6887	0.1722	
pH	2	1.4830	0.3710	0.2580
	4	0.7230	0.1810	
	6.45	0.7920	0.1980	
	10	0.4510	0.1130	
Irradiation intensity ($\mu W/cm^2$)	0	0.5263	0.1315	0.1810
	7.7	1.2500	0.3125	
	11.1	1.1809	0.2952	
	14.8	1.0073	0.2518	
Influence factor sequence (in the order from high to low influence on dye degradation efficiency)	pH, irradiation intensity, dye concentration, H_2O_2 concentration, catalyst dosage			

[a] **K** is the sum of reaction kinetics (k) in the same factor, for example in the 10 ppm dye concentration factor, **K** = 0.0976 + 0.1684 + 0.2629 + 0.0574 (Table 2). K_{avg} is the average value of K. **R** is the range analysis of K_{avg} for each influential parameter.

following operating parameters: dye concentration, catalyst dosage, H_2O_2 concentration, pH, and irradiation intensity. In order to study the effect of these parameters during the Fenton-like degradation, regarding the values of reaction kinetics (k) as the reference standard, an orthogonal design matrix $L_{16}(4^5)$ was performed [48]. The obtained results are presented in this work. The equation of the kinetic model is shown as:

$$ln(C_0/C) = k_{obs}t \quad (2)$$

where k_{obs} is the kinetic rate constant; C_0 is the original concentration of dye; C is the dye concentration at time t.

In orthogonal design matrix $L_{16}(4^5)$ method, reaction kinetics (k) is regarded as the target. Dye concentration, catalyst dosage, H_2O_2 concentration, pH, and irradiation intensity are the key parameters significantly influencing over the outcome of the experiments. Each of these five parameters was varied across a range of four representative values. The experiments were conducted a number of times, enabling each of the five parameters to be adjusted in turn across their respective ranges of four values. The results of the orthogonal arrays $L_{16}(4^5)$ for the synthetic effect of the dye degradation are shown in Table 2, the range of dye concentration is: 10–100 ppm, of catalyst dosage is: 0.2–2.0 g/L, of H_2O_2 concentration is: 0.2–1.0 M, of pH is: 2–10, and of irradiation intensity is: 0–14.8 $\mu W/cm^2$, respectively. The control parameters sequences were calculated by conducting a range analysis. Table 3 shows the results of the range analysis for reaction kinetics (k). As seen from Table 3, the results of the range analysis for control parameter sequence of reaction kinetics (k) are 0.1680, 0.0621, 0.1625, 0.2580, and 0.1810 respectively. These results indicate that the reaction kinetics (k) in the order from high to low dye degradation efficiency is as pH, irradiation intensity, dye concentration, H_2O_2 concentration, catalyst dosage.

Fig. 4 shows the color removal of BR3B-A dye under the irradiation of UV–vis light at different time intervals. At the maximum absorbance peak λ_{max} = 517 nm in the visible light region, the intensity of peaks decreases gradually with the irradiation time. After 5 min irradiation, the maximum absorbance is invisible in the

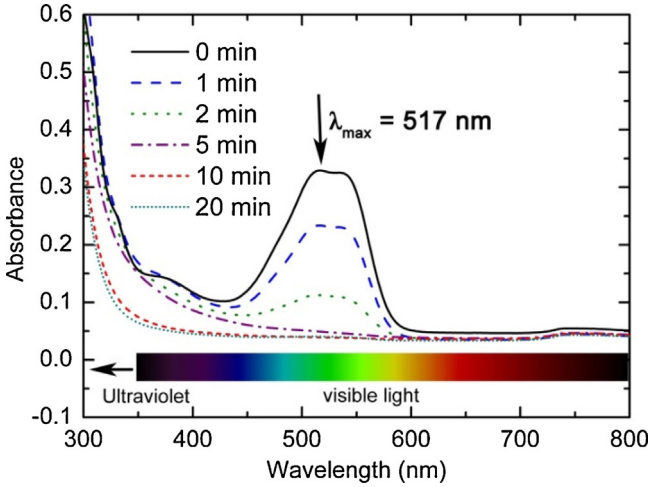

Fig. 4. UV–vis spectra of color removals at 2.0 g/L $Fe_{78}Si_9B_{13}$ dosage within different time intervals (irradiation intensity: 7.7 $\mu W/cm^2$, dye concentration: 20 ppm, pH 2).

spectra. This result suggests that the azo bond (—N=N—) is rapidly cleaved by hydroxyl radicals (•OH) within 5 min and the final products of dye degradation are H_2O, CO_2, NO^{3-}, and SO_4^{2-}, which is in good agreement with the increase of C and S on the recycled ribbon surface in Fig. 3. Fig. 5 shows the progressive color change in BR3B-A dye at different time intervals during photodegradation, according to the control parameter sequence of reaction rate (k) from Table 3. As seen in Fig. 5(a and b), the solutions are almost colorless after 5 min at pH 2; whereas 30 min is required at natural pH 6.45 to achieve the same clarity. In addition, by increasing the irradiation intensity from 0 to 7.7 $\mu W/cm^2$, the dye degradation efficiency is also significantly enhanced (Fig. 5(b) and (c)). It is clear that both the pH of the solution and the irradiation intensity strongly influence the reaction rates (k) according to the calculations of Table 3. In order to study the reaction mechanism, the effect of varying a single parameter was also examined and the obtained results are presented in Section 3.3.

3.3. Single parameter effect on dye degradation

3.3.1. Effect of H_2O_2 concentration

The initial concentration of H_2O_2 is a key parameter in the Fenton-like reactions. Hence, the degradation of BR3B-A dye by $Fe_{78}Si_9B_{13}$ ribbons was initially conducted at natural pH 6.45 and at 20 ppm of dye concentration in order to determine the effect of H_2O_2 concentration. Fig. 6(a) shows the obtained results. It is found that $Fe_{78}Si_9B_{13}$ ribbons without H_2O_2 are incapable of effectively degrading BR3B-A dye: only 52% color removal is achieved at 2.0 g/L dosage of $Fe_{78}Si_9B_{13}$ ribbons. It is postulated that the poor performance is a consequence of the chromophore (—N=N—) bond being poorly degraded by only $Fe_{78}Si_9B_{13}$ ribbons, the color removal in this issue is the adsorption property of the ribbons (Fig. 6(b)). Hydroxyl radicals (•OH) is the primary substance to degrade dye, and it is produced after the addition of H_2O_2. As seen from Fig. 6(a), the color removal rate increases as increasing the H_2O_2 concentration up to 0.5 M. However, further increasing the H_2O_2 concentration from 0.5 M to 1.0 M reduces the color removal rate. The dye solutions of 20 ppm concentration are more than 90% decolorized after only 10 min at 0.5 M H_2O_2. In contrast, for the more highly concentrated H_2O_2 solutions of 0.8 M and 1.0 M, the decolorization achieved is only 76% and 73% respectively after 10 min irradiation.

Table 2
Establishment of the experimental orthogonal arrays $L_{16}(4^5)$.

Exp. *No.*	Dye concentration (ppm)	Catalyst dosage (g/L)	H_2O_2 concentration (M)	pH	Irradiation intensity ($\mu W/cm^2$)	Pseudo-first-order (k)	R^2
1	10	0.2	0.2	2	0	0.0976	0.9937
2	10	0.5	0.5	4	7.7	0.1684	0.9948
3	10	1.0	0.8	6.45	11.1	0.2629	0.9865
4	10	2.0	1.0	10	14.8	0.0574	0.9928
5	20	0.2	0.5	6.45	14.8	0.2910	0.9908
6	20	0.5	0.2	10	11.1	0.1330	0.9913
7	20	1.0	1.0	2	7.7	0.3259	0.9917
8	20	2.0	0.8	4	0	0.1705	0.9907
9	50	0.2	0.8	10	7.7	0.1767	0.9909
10	50	0.5	1.0	6.45	0	0.1742	0.9827
11	50	1.0	0.2	4	14.8	0.2533	0.9902
12	50	2.0	0.5	2	11.1	0.6538	0.9959
13	100	0.2	1.0	4	11.1	0.1312	0.9866
14	100	0.5	0.8	2	14.8	0.4056	0.9825
15	100	1.0	0.5	10	0	0.0840	0.9841
16	100	2.0	0.2	6.45	7.7	0.0634	0.9904

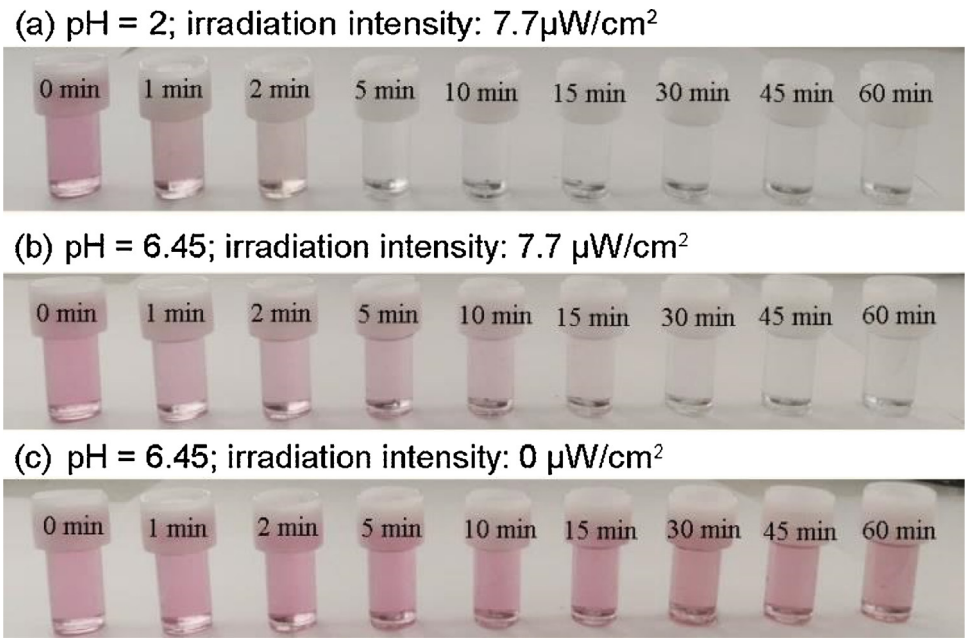

Fig. 5. Visible color change in the BR3B-A dye solution during photo-enhanced Fenton degradation (dye concentration: 20 ppm, $Fe_{78}Si_9B_{13}$ dosage: 2.0 g/L, H_2O_2 concentration: 0.5 M).

The postulated reaction mechanisms for the H_2O_2 modified photo-enhanced Fenton-like reaction is shown below (for 0–0.5 M concentrations):

$$Fe^0 + H_2O_2 \rightarrow Fe^{2+} + 2OH^- \quad (3)$$

$$Fe^{2+} + H_2O_2 \rightarrow Fe^{3+} + OH^- + {}^\bullet OH \quad (4)$$

$${}^\bullet OH + organics \rightarrow products \quad (5)$$

The hydroxyl radical (•OH) is the primary oxidant employed in the degradation of BR3B-A dye. In addition, the conduct of the dye degradation process is most likely to be a surface-catalyzed reaction. The dye molecules are initially adsorbed on the surfaces of the $Fe_{78}Si_9B_{13}$ ribbons and then to be degraded by the generated •OH. As seen from Fig. 6(b), the quantity of adsorption Q_{max} on the surface is 21.9 μmol/g. Further increases the dye concentration from 20 ppm to 30 ppm has no obvious impact on the quantity of dye adsorption, which means the adsorbed dye molecules on the $Fe_{78}Si_9B_{13}$ surface is saturated. The equation of the dye adsorption standard method is shown as:

$$Q = (C_0 - C)V/M \quad (6)$$

where Q is the quantity of absorbance (μmol/g), C_0 and C are the initial concentration and the balanced adsorption concentration, respectively (μmol/L), V is the volume of the dye solution (L), and M is the mass of $Fe_{78}Si_9B_{13}$ (g).

The color removal rate is primarily related to the concentration of the •OH generated during the reaction. As seen from Eqs. (3) and (4), increasing the concentration of H_2O_2 from 0 to 0.5 M promotes the generation of •OH [49], which is attributed to its oxidization potential reacted with the chromophore (—N=N—) in the dye to generate the final products. However, any further addition of H_2O_2 is found to decline the overall reaction rate owing to the formation of penetrative $^\bullet HO_2$ radicals [50] and the excess H_2O_2 being used as •OH scavenger [51,52], as described by:

$${}^\bullet OH + H_2O_2 \rightarrow {}^\bullet HO_2 + H_2O \quad (7)$$

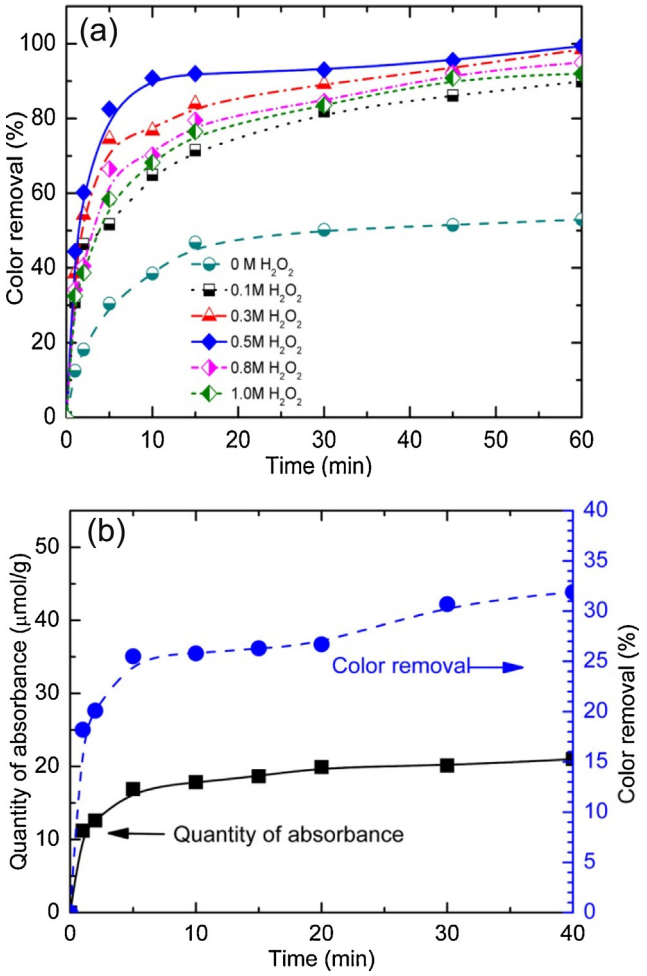

Fig. 6. (a) Effect of H_2O_2 concentration on color removal in percentage *vs.* time ($Fe_{78}Si_9B_{13}$ dosage: 2.0 g/L, irradiation intensity: 7.7 μW/cm^2, dye concentration: 20 ppm, natural pH) and (b) quantity of absorbance and color removal in percentage of BR3B-A dye solution with time in equilibrium, dark conditions (dye concentration: 20 ppm, dosage: 0.3 g/L, natural pH 6.45).

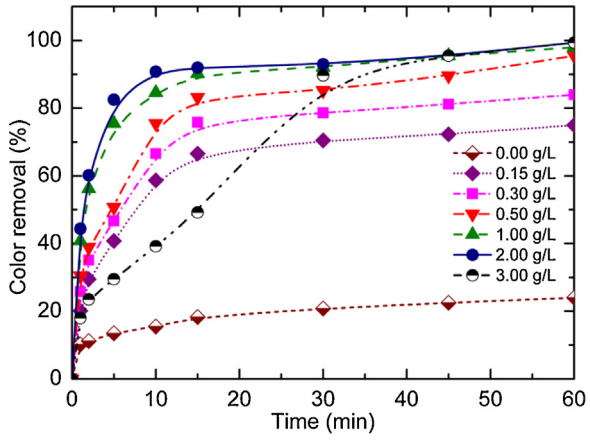

Fig. 7. Color removal as a function of $Fe_{78}Si_9B_{13}$ dosage (H_2O_2 concentration: 0.5 M, irradiation intensity: 7.7 μW/cm^2, dye concentration: 20 ppm, pH 6.45).

3.3.2. *Effect of $Fe_{78}Si_9B_{13}$ ribbon dosage*

Fig. 7 shows the effect of $Fe_{78}Si_9B_{13}$ dosage on the color removal of BR3B-A dye under the following experimental conditions: H_2O_2 concentration of 0.5 M, irradiation intensity of 7.7 μW/cm^2, dye concentration of 20 ppm and natural pH 6.45. H_2O_2 could not effectively degrade BR3B-A dye without the addition of $Fe_{78}Si_9B_{13}$ ribbons; the color removal rate is only 22% after 60 min irradiation. Altering the dosage of $Fe_{78}Si_9B_{13}$ significantly influences the color removal rate. In terms of color removal, 2.0 g/L in this work is a near optimal $Fe_{78}Si_9B_{13}$ dosage for degrading BR3B-A dye. The color removal rate increases sharply as increasing the dosages of $Fe_{78}Si_9B_{13}$ from 0 to 1.0 g/L, and it slightly increases with further increasing the dosages of $Fe_{78}Si_9B_{13}$ from 1.0 to 2.0 g/L. Further increasing the dosages of $Fe_{78}Si_9B_{13}$ to 3.0 g/L can accelerate the decomposition of H_2O_2 to •OH due to the presence of more concentration of Fe^{2+} [53], which results in a slow dye degradation rate as shown in Fig. 7. The sharp increase in color removal rate when the dosage of $Fe_{78}Si_9B_{13}$ is increased from 0 to 1.0 g/L is attributed to that the increased number of Fe^{2+} ions could in turn accelerate the production of •OH, resulting in a rapid degradation of the dye molecules on the surface of the catalyst (Eqs. (3) and (4)). It is further postulated that the slight enhancement in color removal rate resulting from the increase in the dosage of $Fe_{78}Si_9B_{13}$ from 1.0 to 2.0 g/L is ascribed to that the Fe^{3+} ions can revert back to Fe^{2+} *via* alternative mechanisms shown in Eqs. (8) and (9).

$$Fe^{3+} + H_2O_2 \rightarrow Fe^{2+} + {}^{\bullet}HO_2 + H^+ \quad (8)$$

$$Fe^{3+} + {}^{\bullet}HO_2 \rightarrow Fe^{2+} + O_2 + H^+ \quad (9)$$

The reversion cycle of $Fe^{2+} \rightarrow Fe^{3+} \rightarrow Fe^{2+}$ continuously generates •OH, provided that the concentration of •OH in the system is sufficient. However, further increasing the $Fe_{78}Si_9B_{13}$ dosage above 2.0 g/L generates excessive Fe^{3+} irons, which work possibly against the decolorization of the solution by eliminating H_2O_2 from the system.

Table 4
Color removal and reaction kinetics (k) under different pH value ($Fe_{78}Si_9B_{13}$ dosage: 2.0 g/L, H_2O_2 concentration: 0.5 M, irradiation intensity: 7.7 μW/cm^2, dye concentration: 20 ppm).

pH	Color removal (%) at 2 min	Color removal (%) at 10 min	Reaction kinetics (k)	R^2
2	80.4	100	0.7169	0.9997
4	72.5	98.3	0.5588	0.9995
6.45 (natural)	60.2	92.1	0.3116	0.9877
8	46.6	72.4	0.1965	0.9885
10	38.5	65.4	0.1321	0.9832
12	25.8	50.8	0.0747	0.9841

3.3.3. *Effect of pH*

Fig. 8(a) shows the effect of the solution pH values on the color removal and degradation rates of the solutions with pH ranging from 2 to 12. It is observed that both color removal and the reaction kinetics (k) are more sensitive under acid conditions. The optimum pH of the solution is within the range between 2–6, where more than 90% color removal could be achieved after 10 min. Table 4 shows the color removal at 2 min, 10 min and the reaction kinetics (k) under different pH value (the color removal in first 10 min has significant relationship with the reaction kinetics (k), thus, all the tables hereafter only show the color removal at 2 min and 10 min). The degradation rate of BR3B-A dye decreases in conjunction with the increase in pH value. The reason for the improved performance under acid conditions is that the •OH can be effectively produced between the reaction of Fe and H_2O_2 at acid conditions, providing sufficient •OH to degrade and mineralize the dye molecules in the solution. In contrast, the decrease in the degradation efficiency and rate of decolorization in an alkaline solution is owing to ferric precipitation as ferric hydroxide overlaying the surface of the $Fe_{78}Si_9B_{13}$ ribbons and inhibiting the generation of •OH, and also the formation of ferric hydroxide results in a large amount of Fe loss on the ribbon surfaces. A significant mineralization of

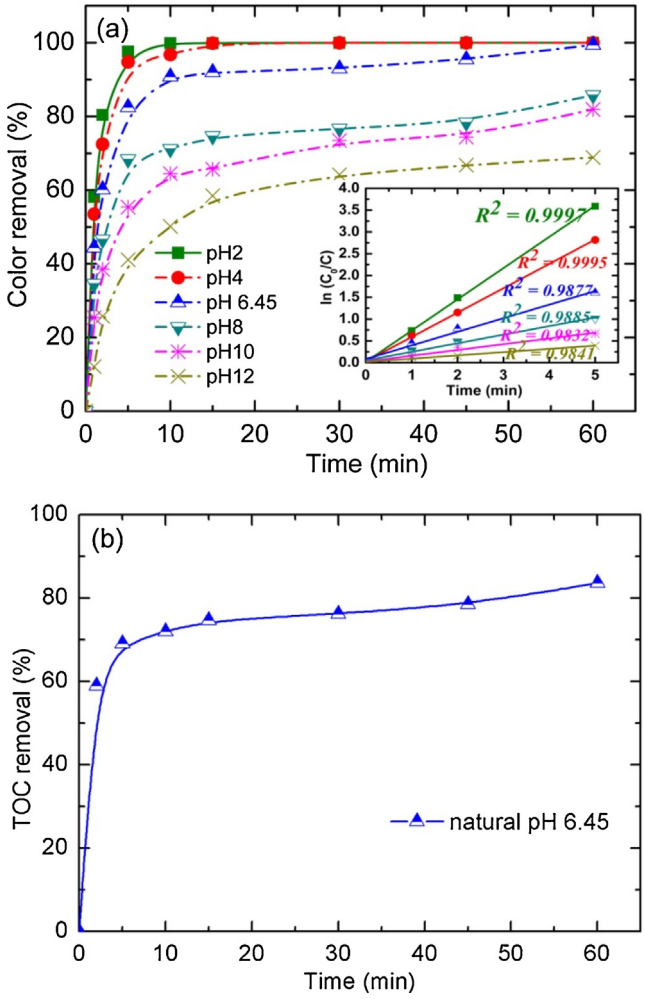

Fig. 8. (a) Effect of pH value on color removal: color removal in percentage *vs.* time at different pH value, (inset) variation of ln (C_0/C) *vs.* time at different pH value; (b) TOC removal during 60 min photo-enhanced degradation at natural pH 6.45 ($Fe_{78}Si_9B_{13}$ dosage: 2.0 g/L, H_2O_2 concentration: 0.5 M, irradiation intensity: 7.7 μW/cm^2, dye concentration: 20 ppm).

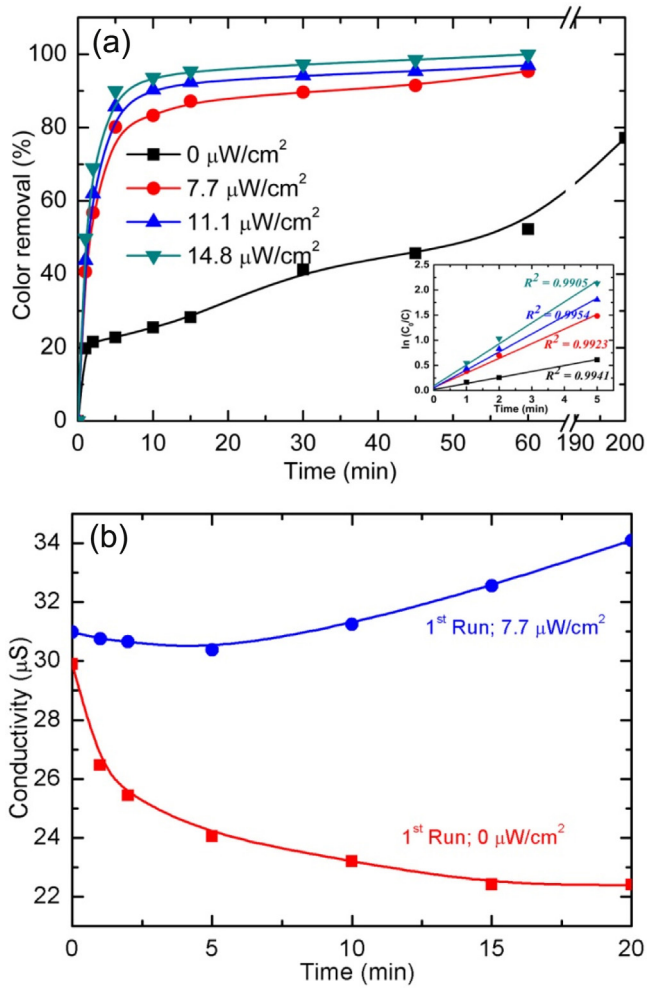

Fig. 9. (a) Effect of irradiation intensity on color removal in percentage *vs.* time, with inset showing the variation of ln (C_0/C) *vs.* time at different irradiation intensity, and (b) Changes of the conductivity of the sample solution during photo-enhanced degradation ($Fe_{78}Si_9B_{13}$ dosage: 2.0 g/L, H_2O_2 concentration: 0.5 M, dye concentration: 20 ppm, pH natural 6.45).

BR3B-A dye in terms of removal of TOC from the dye aqueous solution is shown in Fig. 8(b). It is observed that the dye mineralization is always slower than the dye decolorization (Fig. 8(a)), *i.e.* 59.0% TOC removal at 2 min and 83.6% TOC removal at 60 min at natural pH *vs.* the achieved decolorizations of 61.0% at 2 min and 99.4% at 60 min, respectively. It is certainly because of the by-products are produced during the dye degradation thereby requiring a longer irradiation exposure under UV–vis light.

3.3.4. *Effect of light intensity*

The effect of irradiation intensity on color removal and the degradation rates of BR3B-A dye by photo-enhanced Fenton-like reactions are shown in Fig. 9(a). It is observed that, when the irradiation intensity is increased from 0 to 7.7 μW/cm^2, the overall color removal increases significantly from 78% at 200 min to 98% at 60 min. Further increasing the irradiation intensity from 11.1 to 14.8 μW/cm^2 only slightly enhances the color removal and rate of decolorization. As seen from Fig. 9(a), at irradiation intensity of 11.1 μW/cm^2 or higher, the color removal obtained is more than 80% and the reaction kinetics (k) is higher than 0.2901. In contrast, only 60.2% decolorization of the dye solution at a reaction kinetics (k) of 0.1193 is achieved without irradiation (Table 5 and Fig. 9(a) inset). Therefore, the light irradiation enhances the rate of the photo-enhanced Fenton-like process. This is mainly attributed

Table 5
Color removal rate and reaction kinetics under various values of irradiation intensity ($Fe_{78}Si_9B_{13}$ dosage: 2.0 g/L, H_2O_2 concentration: 0.5 M, dye concentration: 20 ppm, pH natural 6.45).

Light intensity (μW/cm^2)	Color removal (%) at 2 min	Color removal (%) at 10 min	Reaction kinetics (k)	R^2
0	22.8	28.5	0.0413	0.9941
7.7	56.8	83.5	0.2901	0.9923
11.1	62	89.9	0.3558	0.9954
14.8	69	94.1	0.4171	0.9905

to the regeneration of Fe^{2+} by the photochemical effect of light and the concurrent generation of the •OH radicals in the system (Eq. (10)).

$$Fe^{3+} + H_2O + Uv \rightarrow {}^{\bullet}OH + Fe^{2+} + H^+ \quad (10)$$

Fig. 9(b) shows the changes in the conductivity of the sample solution during the BR3B-A dye degradation. The conductivity of the solution without light irradiation decreases in the first 5 min, from 30 μS/cm to 24 μS/cm. In contrast, when the irradiation intensity increases from 0 to 7.7 μW/cm^2, the conductivity of the solution increases continuously, in conjunction with the irradiation time, from 31 μS/cm at 0 min to 34 μS/cm at 20 min. It is

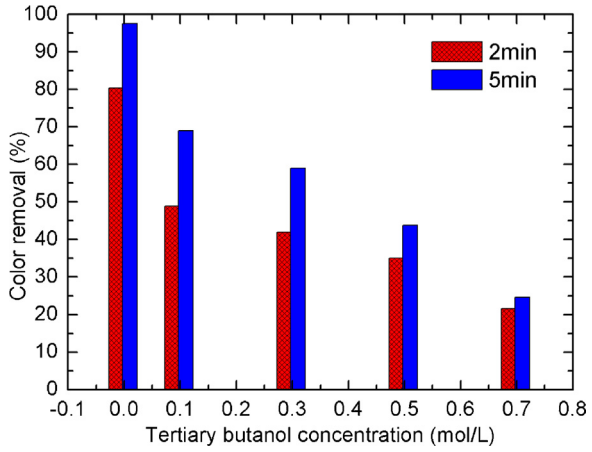

Fig. 10. Effect of tertiary butanol concentration on dye color removal (dye concentration: 20 ppm, pH 2, $Fe_{78}Si_9B_{13}$ dosage: 2.0 g/L, H_2O_2 concentration: 0.5 M, irradiation intensity: 7.7 μW/cm^2).

evidenced that the regeneration of Fe^{2+} is strongly influenced by irradiation intensity [54,55], which is in good agreement with the color removal and reaction kinetics (k) in Fig. 9(a) and also with the dye degradation in terms of color change during photodegradation in Fig. 5.

3.3.5. *Effect of tertiary butanol concentration*

Fig. 10 shows the effect of tertiary butanol concentration on BR3B-A dye color removal. It is observed that the color removal rate decreases sharply after adding tertiary butanol, from 80.4% color removal at 2 min and 97.6% color removal at 5 min of 0 mol/L tertiary butanol concentration (pH 2), down to 21.6% color removal at 2 min and 24.6% color removal at 5 min of 0.7 mol/L tertiary butanol concentration, respectively. In addition, the color removal rate increases very slightly between 2 min and 5 min under 0.7 mol/L tertiary butanol concentration, providing an increase of color removal of only 3% at 0.7 mol/L tertiary butanol compared with an increase of color removal of 17% at 0 mol/L tertiary butanol concentration. These results indicate that the primary active species •OH is eliminated very quickly after adding tertiary butanol (a scavenger of •OH) [56,57], leaving behind a dramatically reduced supply of •OH in the solution for degrading the BR3B-A dye molecules.

3.4. *Recycled ribbons*

Multiple dye degradation cycles using the same $Fe_{78}Si_9B_{13}$ ribbon catalysts were carried out in order to study the color removal efficiency, the reaction kinetics (k), and the changes in conductivity and pH during the photodegradation process. The results of the multiple processing cycles using the same ribbons are shown in Fig. 11. As seen from Fig. 11(a) and (b), reusing the catalyst slightly reduces the rate of color removal and the reaction kinetics (k) after 4 cycles of use. After 20 min irradiation, the color removal drops from 90% at a reaction kinetic (k) of 0.2038 for the 1st run down to 70% for color removal and 0.0469 respectively for a reaction kinetic (k) for the 4th run. The slight reduced catalytic capacity of $Fe_{78}Si_9B_{13}$ ribbons could be attributed to the presence of crystallized α-Fe, iron oxide, and SiO_2 on the ribbon surfaces during dye degradation (Fig. 2 and Fig. 3) and the adsorption property of the ribbons being influenced by the generation of intermediates during dye degradation process [53]. A series of photo-enhanced Fenton-like degradation experiments were carried out in order to measure the pH and the conductivity of the solution with various durations of irradiation. For these experiments, a BR3B-A dye concentration of 20 ppm and catalyst dosage of 2.0 g/L $Fe_{78}Si_9B_{13}$ were used, with

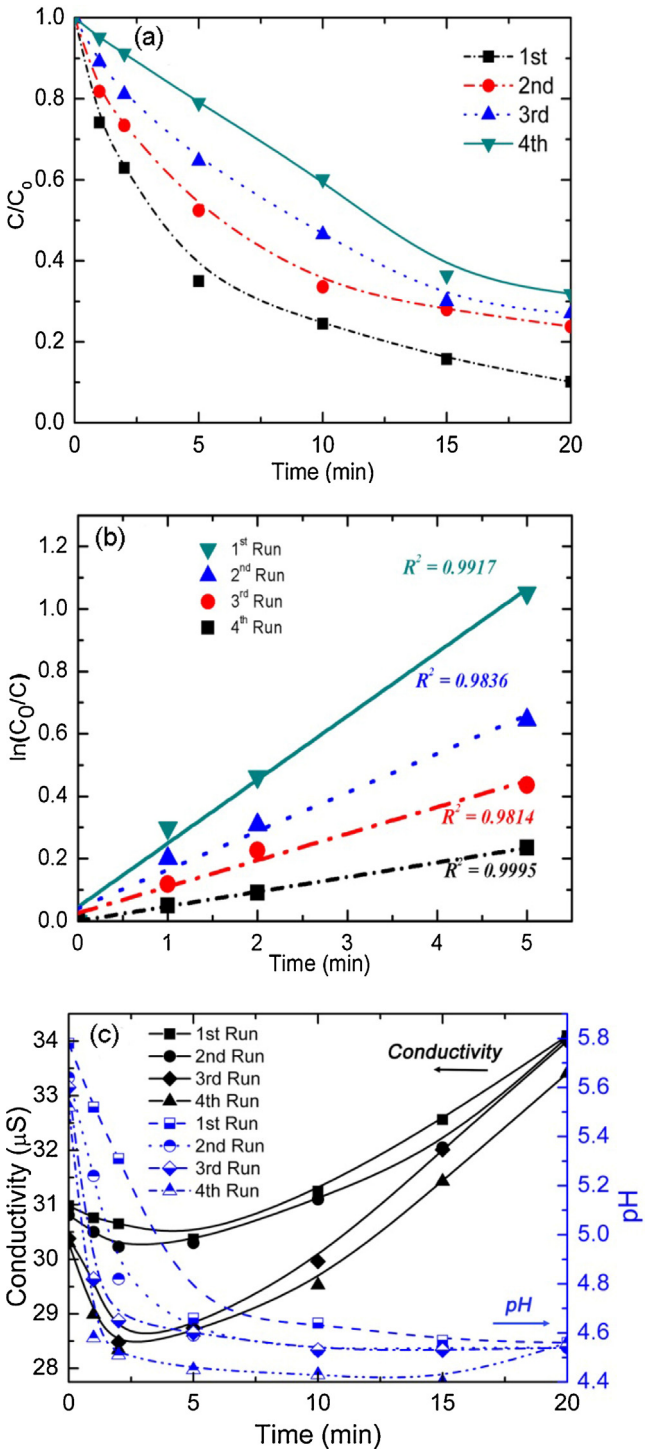

Fig. 11. (a) Photo-enhanced Fenton-like degradation of BR3B-A dye with reused amorphous $Fe_{78}Si_9B_{13}$ ribbons, (b) variation of ln (C_0/C) *vs.* time of reused $Fe_{78}Si_9B_{13}$ ribbons, and (c) changes in the pH and conductivity of the sample solution with reused $Fe_{78}Si_9B_{13}$ ribbons under UV–vis light (dye concentration: 20 ppm; natural pH 6.45; $Fe_{78}Si_9B_{13}$ dosage: 2.0 g/L; H_2O_2 concentration: 0.5 M; irradiation intensity: 7.7 μW/cm^2).

results being presented in Fig. 11(c). The initial pH and conductivity of the solution decrease with increasing number of cycle times that the $Fe_{78}Si_9B_{13}$ catalyst ribbons were used. Although the ribbon surfaces have been slightly decayed (α-Fe, iron oxide, and SiO_2), the ribbons still demonstrate acceptable catalytic performance after 4 uses, removing more than 70% of the color within 20 min (Table 6). During the first run of the experiment, the initial pH of the aqueous

Table 6
Color removal and reaction kinetics of reused $Fe_{78}Si_9B_{13}$ ribbons (dye concentration: 20 ppm; natural pH 6.45; $Fe_{78}Si_9B_{13}$ dosage: 2.0 g/L; H_2O_2 concentration: 0.5 M; irradiation intensity: 7.7 μW/cm^2).

Recycled times	Color removal (%) at 10 min	Color removal (%) at 20 min	Reaction kinetics (k)	R^2
1st Run	78.7	91.2	0.2038	0.9917
2nd Run	70.8	79.3	0.1240	0.9836
3rd Run	59.9	77.2	0.0849	0.9814
4th Run	47.7	72.3	0.0469	0.9995

solution is 5.78 after adding H_2O_2. As observed in Fig. 11(c), the pH of the solution drops sharply during the first 5 min, decreasing from 5.78 at 0 min to 4.71 at 5 min of the 1st run, whereas the reaction kinetics (k) is 0.2038 (Table 6). After 5 min, the pH changed much more slowly, dropping to 4.57 after 20 min. The likely reason for the change in pH is the formation of acid products (H^+) during the photo-enhanced Fenton-like reaction (Eq. (8) and Eq. (9)) and the increase in conductivity after 2 min irradiation time [54]. The slowing down of the pH changing indicates that the dye is fast degraded in the first 5 min due to the short-life of •OH [10]. In addition, the conductivity of the solution drops slightly when irradiated from 0 to 2 min, which is likely evidence that this is a surface-catalyzed reaction [53].

4. Conclusion

It is clear from the results of the proposed photo-enhanced Fenton-like dye degradation process that amorphous $Fe_{78}Si_9B_{13}$ ribbons are a very promising catalyst for use in industrial wastewater treatment. In this work, the individual and combined effects of the various reaction parameters were investigated by employing an orthogonal matrix ($L_{16}(4^5)$) experimental methodology. It is found that the ranked order of the reaction parameters from those having the most impact on the reaction rate to those having the least is as follows: pH, irradiation intensity, dye concentration, H_2O_2 concentration, and catalyst dosage.

By using the photo-enhanced Fenton-like process, nearly 100% of the dye colorant can be removed, at a reaction kinetic (k) of 0.7169 after only 5 min with pH 2. The intensity of the irradiation also has a significant impact on the color removal and reaction kinetics (k). Increasing the irradiation intensity from 0 to 14.8 μW/cm^2 promotes color removal of the solution from 60.2% to 94.1% and enhances the reaction kinetics (k) from 0.1193 to 0.4171. The mineralization of dye solution characterized by TOC removal at natural pH 6.45 and the investigation of the production of •OH captured by tertiary butanol indicate that the dye molecules can be effectively degraded and mineralized by the production of •OH during this Fenton-like process. Microstructural characterizations of the as-received amorphous $Fe_{78}Si_9B_{13}$ ribbon confirm its amorphous state. Detailed characterizations of the reused $Fe_{78}Si_9B_{13}$ ribbons by XRD, UV–vis DRS, SEM and EDS reveal that the precipitated substances on the ribbon surface are α-Fe, iron oxides and SiO_2. These precipitations cause a slightly increased decay of the ribbon surface. Nevertheless, the amorphous ribbons still exhibit good stability and photocatalytic performace, demonstrating the prospect of further reusability.

In this study, the proposed photo-enhanced Fenton process has demonstrated a dramatic improvement in dye degradation efficiency. These improvements along with other highly desirable properties inherent in the process, such as the low-cost, very stable and highly reusable amorphous $Fe_{78}Si_9B_{13}$ ribbons as catalyst, and the rapid reaction kinetics which are achieved, provide a speedy and environmentally friendly solution for the treatment of industrial wastewater.

Acknowledgements

The authors appreciate Mr. Jian Kang for the measurements of TOC, Professor Hongqi Sun for the constructive discussion, and Mr. Mark Bannister for the supply of concentrated tertiary butanol. Financial supports from the ECU Innovator Awards (Project No. 23641) and Australian Research Council Discovery Project (DP130103592) are gratefully acknowledged.

References

[1] R. Hasegawa, J. Magn. Magn. Mater. 304 (2006) 187–191.
[2] J. Jayaraj, D. Sordelet, D. Kim, Y. Kim, E. Fleury, Corros. Sci. 48 (2006) 950–964.
[3] N. Belhadj Tahar, A. Savall, J. Appl. Electrochem. 29 (1999) 277–283.
[4] J.A. Zazo, J.A. Casas, A.F. Mohedano, J.J. Rodríguez, Appl. Catal B: Environ. 65 (2006) 261–268.
[5] J. Miao, L.C. Zhang, H. Lin, Chem. Eng. Sci. 87 (2013) 152–159.
[6] B. Merzouk, B. Gourich, K. Madani, C. Vial, A. Sekki, Desalination 272 (2011) 246–253.
[7] L. Das, S. Chatterjee, D.B. Naik, S. Adhikari, J. Hazard. Mater. 298 (2015) 19–27.
[8] P.M. Alvárez', F.J. Beltrán, F.J. Masa, J.P. Pocostales, Appl. Catal B: Environ. 92 (2009) 393–400.
[9] K.Y. Foo, B.H. Hameed, J. Hazard. Mater. 175 (2010) 1–11.
[10] J. Miao, Z. Jia, H.B. Lu, D. Habibi, L.C. Zhang, J. Taiwan, Inst. Chem. Eng. 45 (2014) 1636–1641.
[11] Z. Jia, J. Miao, H.B. Lu, D. Habibi, W.C. Zhang, L.C. Zhang, J. Taiwan, Inst. Chem. Eng. 60 (2016) 267–274.
[12] J. Yang, X. Bian, Y. Bai, X. Lv, P. Wang, J. Non-Cryst. Solids 358 (2012) 2571–2574.
[13] B. Lin, X. Bian, P. Wang, G. Luo, Mater. Sci. Eng. B 177 (2012) 92–95.
[14] C. Zhang, Z. Zhu, H. Zhang, Z. Hu, J. Non-Cryst. Solids 358 (2012) 61–64.
[15] C. Zhang, H. Zhang, M. Lv, Z. Hu, J. Non-Cryst. Solids 356 (2010) 1703–1706.
[16] S.H. Joo, A.J. Feitz, T.D. Waite, Environ. Sci. Technol. 38 (2004) 2242–2247.
[17] M. Bayat, M. Sohrabi, S.J. Royaee, J. Ind. Eng. Chem. 18 (2012) 957–962.
[18] J. Fernandez, J. Bandara, J. Kiwi, A. Lopez, P. Albers, Chem. Commun. (1998) 1493–1494.
[19] A. Baiker, Faraday Discuss. Chem. Soc. 87 (1989) 239–251.
[20] W.F. de Souza, I.R. Guimarães, L.C.A. Oliveira, M.C. Guerreiro, A.L.N. Guarieiro, K.T.G. Carvalho, J. Mol. Catal. A: Chem. 278 (2007) 145–151.
[21] J. Bandara, J.A. Mielczarski, A. Lopez, J. Kiwi, Appl. Catal B: Environ. 34 (2001) 321–333.
[22] R.C.C. Costa, M.F.F. Lelis, L.C.A. Oliveira, J.D. Fabris, J.D. Ardisson, R.R.V.A. Rios, C.N. Silva, R.M. Lago, J. Hazard. Mater. 129 (2006) 171–178.
[23] J.H. Ramirez, F.J. Maldonado-Hódar, A.F. Pérez-Cadenas, C. Moreno-Castilla, C.A. Costa, L.M. Madeira, Appl. Catal B: Environ. 75 (2007) 312–323.
[24] M. Cheng, W. Ma, J. Li, Y. Huang, J. Zhao, Y.x. Wen, Y. Xu, Environ. Sci. Technol. 38 (2004) 1569–1575.
[25] J. Feng, X. Hu, P.L. Yue, Water Res. 40 (2006) 641–646.
[26] W.L. Johnson, MRS. Bull. 24 (1999) 42–56.
[27] A. Inoue, Acta. Mater. 48 (2000) 279–306.
[28] C.J. Byrne, M. Eldrup, Science 321 (2008) 502–503.
[29] A. Inoue, A. Takeuchi, Acta. Mater. 59 (2011) 2243–2267.
[30] W.H. Wang, Adv. Mater. 21 (2009) 4524–4544.
[31] J.Q. Wang, Y.H. Liu, M.W. Chen, D.V. Louzguine Luzgin, A. Inoue, J.H. Perepezko, Sci. Rep. 2 (2012).
[32] J.Q. Wang, Y.H. Liu, M.W. Chen, G.Q. Xie, D.V. Louzguine Luzgin, A. Inoue, J.H. Perepezko, Adv. Funct. Mater. 22 (2012) 2567–2570.
[33] S.R. Couto, J.L. Toca Herrera, Biotechnol. Mol. Biol. Rev. 1 (2006) 115–120.
[34] M. Chang, C.R. Overk, I. Kastrati, K.W. Peng, P. Yao, Z.H. Qin, P. Petukhov, J.L. Bolton, G.R. Thatcher, Adv. Exp. Med. Biol. 617 (2008) 601–607.
[35] J. Peralta Hernandez, Y. Meas Vong, F. Rodriguez, T. Chapman, M. Maldonado, L. Godinez, Dyes. Pigm. 76 (2008) 656–662.
[36] B. Barragan, C. Costa, M. Marquez, Dyes. Pigm. 75 (2007) 73–81.
[37] K. Yogendra, N. Suneel, K. Mahadevan, N. Madhusudhana, Int. J. Environ. Sci. Res. 1 (2011) 11–15.
[38] Z.H. Lai, Y.S. Chao, H. Conrad, K. Chu, J. Mater. Res. 10 (1995) 900–906.
[39] L.C. Zhang, Z.Q. Shen, J. Xu, Mater. Sci. Eng. A. 394 (2005) 204–209.
[40] H.B. Lu, L.C. Zhang, A. Gebert, L. Schultz, J. Alloys Compd. 462 (2008) 60–67.
[41] L.C. Zhang, J. Xu, J. Non-Cryst. Solids 347 (2004) 166–172.
[42] P. Yu, L.C. Zhang, W.Y. Zhang, J. Das, K.B. Kim, J. Eckert, Mater. Sci. Eng. A. 444 (2007) 206–213.
[43] M. Calin, L.C. Zhang, J. Eckert, Scripta Mater. 57 (2007) 1101–1104.
[44] Y. Ma, B. Rheingans, F. Liu, E. Mittemeijer, J. Mater. Sci. 48 (2013) 5596–5606.
[45] C.M. Huang, G.T. Pan, Y.C.M. Li, M.H. Li, T.C.K. Yang, Appl. Catal A: Gen. 358 (2009) 164–172.
[46] K. Sun, H. Xia, E. Hensen, R. van Santen, C. Li, J. Catal. 238 (2006) 186–195.
[47] J. Pérez-Ramírez, J. Catal. 227 (2004) 512–522.

[48] I. Arslan Alaton, N. Ayten, T. Olmez Hanci, Appl. Catal B: Environ. 96 (2010) 208–217.
[49] R. Prihod'ko, I. Stolyarova, G. Gündüz, O. Taran, S. Yashnik, V. Parmon, V. Goncharuk, Appl. Catal B: Environ. 104 (2011) 201–210.
[50] M. Chong, B. Jin, C. Chow, C. Saint, Water. Res. 44 (2010) 2997–3027.
[51] C. Jiang, S. Pang, F. Ouyang, J. Ma, J. Jiang, J. Hazard. Mater. 174 (2010) 813–817.
[52] X. Wang, Y. Pan, Z. Zhu, J. Wu, Chemosphere 117 (2014) 638–643.
[53] L. Wang, Y. Yao, Z. Zhang, L. Sun, W. Lu, W. Chen, H. Chen, Chem. Eng. J. 251 (2014) 348–354.
[54] M. Stylidi, D.I. Kondarides, X.E. Verykios, Appl. Catal B: Environ. 40 (2003) 271–286.
[55] Z. He, L. Lin, S. Song, M. Xia, L. Xu, H. Ying, J. Chen, Sep. Purif. Technol. 62 (2008) 376–381.
[56] I. Stranic, G.A. Pang, R.K. Hanson, D.M. Golden, C.T. Bowman, J. Phys. Chem. A 117 (2013) 4777–4784.
[57] T. Zhou, Y. Li, J. Ji, F.-S. Wong, X. Lu, Sep. Purif. Technol. 62 (2008) 551–558.